JACS
JOURNAL OF THE AMERICAN CHEMICAL SOCIETY
Article
pubs.acs.org/JACS

Integration of Intrinsic Proton Conduction and Guest-Accessible Nanospace into a Coordination Polymer

Daiki Umeyama,[†] Satoshi Horike,*[,†,‡] Munehiro Inukai,[§] and Susumu Kitagawa*[,†,§]

[†]Department of Synthetic Chemistry and Biological Chemistry, Graduate School of Engineering, Kyoto University, Katsura, Nishikyo-ku, Kyoto 615-8510, Japan

[‡]Japan Science and Technology Agency, PRESTO, 4-1-8 Honcho, Kawaguchi, Saitama 332-0012, Japan

[§]Institute for Integrated Cell-Material Sciences (WPI-iCeMS), Kyoto University, Yoshida, Sakyo-ku, Kyoto 606-8501, Japan

Supporting Information

ABSTRACT: We report the synthesis and characterization of a coordination polymer that exhibits both intrinsic proton conductivity and gas adsorption. The coordination polymer, consisting of zinc ions, benzimidazole, and orthophosphate, exhibits a degree of flexibility in that it adopts different structures before and after dehydration. The dehydrated form shows higher intrinsic proton conductivity than the original form, reaching as high as 1.3×10^{-3} S cm^{-1} at 120 °C. We found that the rearranged conduction path and liquid-like behavior of benzimidazole molecules in the channel of the framework afforded the high proton conductivity. Of the two forms of the framework, only the dehydrated form is porous to methanol and demonstrates guest-accessible space in the structure. The proton conductivity of the dehydrated form increases by 24 times as a result of the in situ adsorption of methanol molecules, demonstrating the dual functionality of the framework. NMR studies revealed a hydrogen-bond interaction between the framework and methanol, which enables the modulation of proton conductivity within the framework.

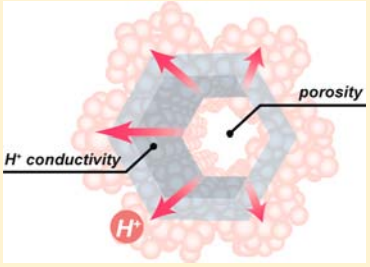

INTRODUCTION

Solid state proton (H^+) conductors are an important class of materials for energy conversion in fuel cells, hydrogen sensing, and electrochemical production of hydrogen.[1] Whereas most researches focus on proton conductivity value, the integration of proton conductivity and other functions in these materials is challenging in terms of both synthesis and applications. For example, dual-function proton conductors with guest-accessible space (porosity) are potentially useful as sensors and catalysts. However, a dense, nonporous structure is more preferable for proton conduction, where proton hopping sites are arranged closely.[2,1c] Therefore, integration of these two contradictory functions, proton conductivity and porosity, in a single-phase compound is an interesting concept. To achieve such dual functionality, we must construct a stable porous structure that also has intrinsic proton conductivity.

Recently, coordination polymers (CPs) and metal−organic frameworks (MOFs) have received attention as proton-conducting materials.[3] CPs are constructed of metal ions and bridging ligands and have various structures and diverse chemical composition.[4] For these porous substances, the main approach for establishing proton conductivity has been to impregnate them with proton carrier molecules, such as H_2O and azoles.[5] In these cases, the frameworks themselves have negligible proton conductivity owing to their highly porous structures and thus cannot achieve dual functionality. On the other hand, we recently developed a synthetic strategy to render intrinsic proton conductivity into nonporous CP frameworks.[6] On the basis of these results, for this study, we sought to achieve dual functionality in a single framework. We show that the use of a proton conductive ligand as well as a bulky template achieves both ion conductivity and porosity. To demonstrate the dual functionality, we also describe the in situ modulation of the proton conductivity of the framework through the adsorption of gaseous molecules into the open pores.

RESULTS AND DISCUSSION

Structures of 1 and 1′. To create a CP with intrinsic proton conductivity and guest-accessible space, we employed a proton conductive ligand (phosphoric acid[7]) as well as a bulky component (benzimidazole, denoted as Hbim). The CP was synthesized by combining these components with zinc oxide. Mechanical milling of zinc oxide, phosphoric acid, and Hbim gave a white crystalline powder (**1**). Single crystal X-ray structural analysis identified the structure and chemical formula of **1** as $[Zn_3(H_2PO_4)_6(H_2O)_3](Hbim)$. The coordination network is composed of three octahedral Zn^{2+} ions with six bridging phosphates and three water molecules coordinated to the zinc ions, to form a one-dimensional (1D) chain of ZnO_6 octahedrons along the *a* axis (Figure 1a).

The infrared (IR) spectrum of **1**, which showed an N−H stretching band almost identical with that of bulk Hbim, suggested that Hbim molecules in **1** are neutral (not protonated or deprotonated) (Figure S1 of the Supporting

Received: May 28, 2013
Published: July 5, 2013

   dx.doi.org/10.1021/ja4051668 | J. Am. Chem. Soc. 2013, 135, 11345−11350

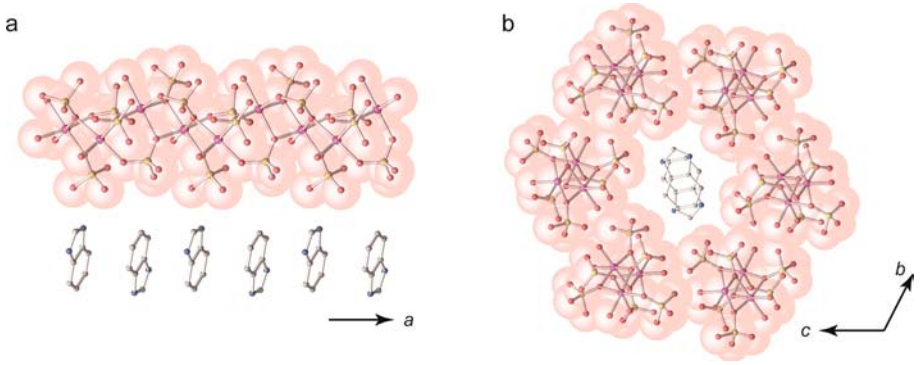

Figure 1. (a) Crystal structure of a 1D coordination chain of **1** along the *a* direction. (b) Packing structure of **1** viewed on the *bc* plain. The atoms Zn, P, O, N, and C, are shown in purple, yellow, red, blue, and gray, respectively. The H atoms have been omitted.

Information, SI). Hence the 1D chains of **1** should also be neutral, which indicates that each phosphate has two protons, making it monoanionic (1−).[8] These 1D chains stack in the *bc* plane in a pattern mediated by hydrogen-bond interactions, and the Hbim molecules locate between these chains such that they are surrounded by six chains and stacked alternately along the *a* axis engaging in $\pi-\pi$ interactions (Figure 1b).

There are two kinds of phosphates in **1**: one type coordinates with two zinc ions via a single bridging oxygen atom (μ_2), and the other coordinates via two oxygen atoms that bridge three zinc ions (μ_3). Of these two forms, only the μ_2-phosphates can contribute to the Grotthuss mechanism because it requires freely rotatable hopping sites,[9,1c] and the rotatable μ_2-phosphates of **1** are isolated from each other (μ_2- and μ_3-phosphates are aligned alternately in the chain, Figure S2 of the SI). The Hbim residue, which is the other rotatable component of **1**, potentially transfers protons by the Grotthuss mechanism. As we explain later, **1** transforms into an alternate structure by releasing coordinated water molecules. We will explain that this transformation provides effective proton-migration pathways as well as porosity, allowing the capture of gaseous methanol.

Thermogravimetric analysis (TGA) of **1** shows a plateau region up to 60 °C, followed by a 5.5% loss of mass through 100 °C (Figure S3 of the SI). The loss corresponds to the release of the three water molecules of **1** (calcd. 5.7%). Dehydrated **1** has the chemical formula $[Zn_3(H_2PO_4)_6](Hbim)$ (denoted as **1′**). The structural transformation from **1** to **1′** during the heating process was monitored by variable-temperature powder X-ray diffraction (VT-PXRD) under flowing N_2. The diffraction patterns mimic the simulated pattern of **1** below 60 °C then diverge above 80 °C (Figure S4 of the SI). On the basis of the TGA result, we attributed this structural change to the dehydration of **1**. Once dehydration occurs, **1′** maintains the same structure over the temperature range from 25 to 140 °C. This indicates that the driving force behind the structural transformation is deformation around the zinc ion, which loses one water molecule from its octahedral (O_h) coordination sphere. **1′** gradually retransforms to the original structure (**1**) under humid condition by capturing water molecules (Figure S4e of the SI). Because **1** loses single crystallinity upon dehydration, we have not obtained a crystal structure of **1′**. Instead, the structure was analyzed using ^{31}P solid-state NMR because the chemical shift of ^{31}P is sensitive to its coordination number and degree of condensation. The degree of condensation is represented as Q^n (n = 0−4), where orthophosphate is Q^0 and fully condensed phosphate is Q^4.[10] The ^{31}P NMR spectrum of **1′** indicates that **1′** maintains the 1D structure of the zinc-phosphate chains and Hbim (Figure S5 of the SI). Spectra taken before and after dehydration reflect the region of Q^0, which suggests that no condensation of phosphates occurs and they remain coordinated to zinc ions after dehydration. However, the shifted peaks of **1′** indicate the coordination environment of some phosphates has changed, which will be discussed later in association with the proton conduction mechanism of **1′**. A Pawley fitting analysis of the powder pattern of **1′** confirmed that **1′** has single-phase purity (Figure S6 of the SI). Although the crystal system is changed from the original triclinic form ($P-1$) to a monoclinic system ($P2_1/c$), the volume per zinc ion is nearly unchanged (232 Å^3 for **1** and 235 Å^3 for **1′**).

Intrinsic Proton Conductivity of 1 and 1′. Having been constructed of proton-conductive components, **1** and **1′** are potentially suitable for proton conduction. Because both structure and acidity strongly influence proton conductivity, slight alterations in structure could result in a totally different mechanism of proton conduction. We measured the proton conductivity of **1** and **1′** by impedance spectroscopy under dry atmospheric N_2. To exclude the effect of gaseous water molecules arising from the dehydration of **1**, we measured the conductivity of **1** from 30 to 60 °C, a range where **1** preserves the coordinated water molecules. The Nyquist plots of **1** show two impedance responses (Figure S7a of the SI). We then used two series of parallel *RQ* circuits to fit the impedance data of **1** (*R* represents a resistance and *Q*, a constant phase element).[11]

We regarded the component in the higher frequency region as bulk resistivity and the one at lower frequency as grain-boundary resistivity.[12] Although **1** has acidic protons in the structure, the conductivity values are low in this temperature region, namely, 1.4×10^{-7} S cm^{-1} at 30 °C and 6.1×10^{-7} S cm^{-1} at 60 °C with the activation energy of 0.4 eV, as seen in the Arrhenius plot (Figure 2). The reason for the low conductivities probably lies in the structure of **1**, where the hydrogen bonds are not continuous (Figure S2a,b of the SI).

We measured the conductivity of **1′** from 30 to 120 °C. We used a single *RQ* component to fit the impedance data because the Nyquist plots of **1′** showed a single impedance response, which we regarded as bulk resistance (Figure S7b of the SI). The reason for the absence of grain boundary is not clear, but the phenomenon is also observed in doped zirconia.[13] The conductivity value at 30 °C is 1.2×10^{-7} S cm^{-1}, which is almost the same as that of **1**. In the Arrhenius plot, however, the conductivity increases rapidly as the temperature rises, reaching 1.5×10^{-5} S cm^{-1} at 60 °C and 1.3×10^{-3} S cm^{-1} at 120 °C (Figure 2). In general, water molecules inside the

dx.doi.org/10.1021/ja4051668 | J. Am. Chem. Soc. 2013, 135, 11345−11350

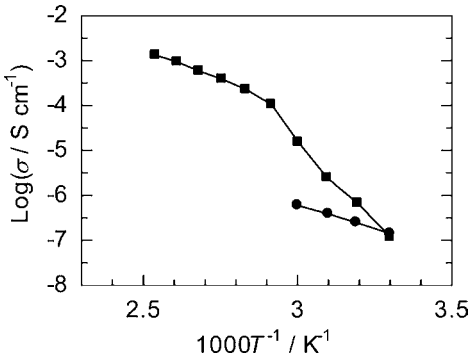

Figure 2. Arrhenius plots of the anhydrous conductivity of **1** (●) and **1′** (■) under atmospheric N_2.

framework function as proton carriers to increase the conductivity.[14] The anomalous improvement in conductivity afforded by the dehydration of **1** indicates that the structural transformation is more significant than the presence of water molecules for enhancing the proton conductivity of **1′**.

Intrinsic Proton Conduction Mechanism of 1′. In contrast to **1**, **1′** has a bend in the Arrhenius plot at 70 °C, suggestive of two distinct conduction mechanisms occurring above and below 70 °C. Since we presumed that the mobility of the phosphate and Hbim moieties were the dominant factors responsible for proton conduction in **1′**, we investigated their motilities by ^{2}H solid-state static NMR. In order to distinguish phosphate and Hbim, we prepared **1′** with deuterated phosphate ($[Zn_3(D_2PO_4)_6](Hbim)$, denoted as **1′**-P-d_2) and with deuterated Hbim ($[Zn_3(H_2PO_4)_6](Hbim\text{-}4,5,6,7\text{-}d_4)$, denoted as **1′**-Hbim-d_4). As shown in Figure 3, parts a and f,

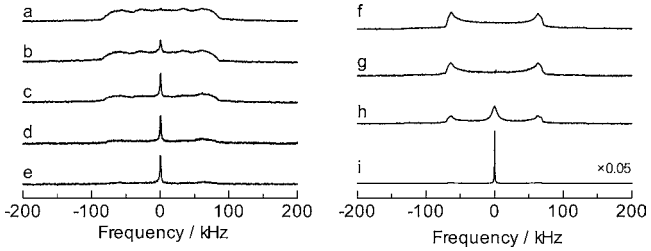

Figure 3. ^{2}H solid-state static NMR spectra of **1′**-P-d_2 at (a) 25 °C, (b) 40 °C, (c) 60 °C, (d) 80 °C, and (e) 100 °C and **1′**-Hbim-d_4 at (f) 25 °C, (g) 50 °C, (h) 75 °C, and (i) 100 °C.

at 25 °C, the NMR spectrum of **1′**-P-d_2 shows an intermediate state between a Pake doublet and an isotropic center peak, whereas **1′**-Hbim-d_4 shows only a Pake doublet. This suggests that the phosphate moiety in **1′** is more mobile than Hbim at 25 °C. Figure 3b,c shows gradual growth of the center peak, indicating increasing mobility of the phosphate moiety. Figure 3g shows a Pake doublet that is almost identical with that in Figure 3f. This indicates that the Hbim moiety in **1′** has similar low mobility at 50 and 25 °C, regardless of the increase in proton conductivity.[15] These observations suggest that the 1D chains of zinc phosphate in **1′** function as the main proton hopping path below 70 °C. Although we have not identified the precise structure of **1′**, this conduction mechanism requires interconnected μ_2-phosphates. The structural transformation from **1** to **1′** is likely critical to the formation of the dynamic hydrogen-bond network.

Above 70 °C, the slope in the Arrhenius plot flattens. In concert with this change in slope, the ^{2}H NMR of **1′**-Hbim-d_4 begins to show an isotropic center peak (Figure 3h). This center peak sharpens dramatically at 100 °C (Figure 3i), while the center peak of **1′**-P-d_2 continues to grow (Figure 3d,e). These spectra suggest that Hbim in **1′** starts rotating randomly above 70 °C, and both the phosphate and Hbim moieties in **1′** have high mobility at 100 °C. The liquid-like behavior of the Hbim residue in the solid channel constructed of 1D zinc phosphate chains is a feature characteristic of coordination-network-based plastic crystals.[6a] The excitation of the rotational motion gives a broad endothermic peak in the differential scanning calorimetry (DSC) spectrum at approximately 60 °C (Figure S8 of the SI). The broadness of the peak indicates the limited cooperativity of the transition, which supports the coexistence of the Pake doublet and isotropic peak in the ^{2}H NMR spectra at high temperature. Hence we conclude that the dynamic Hbim moiety aligned in the channel is also available for proton conduction above 70 °C, which causes the change in the slope (activation energy) of the Arrhenius plot. The transition shows thermal hysteresis and the isotropic motion of benzimidazole is maintained in the cooling process, which is revealed by DSC and Arrhenius plot (Figure S8 and S9 of the SI). Compared to a previous case[6a] where imidazole rotates in an anisotropic manner, the motion of the Hbim residue in **1′** is isotropic in spite of its heavier molecular weight and larger molecular volume. This indicates that **1′** is equipped with enough space for Hbim to rotate freely. The activation energy in the region above 70 °C is 0.5 eV, which is appropriate for the Grotthuss mechanism. The region below 70 °C shows a higher activation energy (1.5 eV), although the mechanism should be the same (Grotthuss) because all phosphates are coordinated to zinc ions. Although we fail to explain the origin of the large activation energy owing to the ambiguous structure of **1′**, possible reasons are discussed in the literature.[16]

Guest-Accessible Space of 1′. The fact that **1** loses the coordinated water molecules around 80 °C (associated with structural change) suggests that **1′** may be capable of capturing some guest molecules. Thus, we then performed a gas adsorption study on **1** and **1′**. We chose methanol as the adsorbate because its dipole moment indicates its potential to interact with the chains of **1** and it is commonly adsorbed in acidic porous materials like zeolites.[17] Figure 4 shows the adsorption and desorption isotherms of methanol in **1** and **1′** measured at 25 °C. As can be seen in the figure, **1** does not adsorb methanol, consistent with its nonporous structure, whereas **1′** adsorbs methanol with hysteresis in the desorption

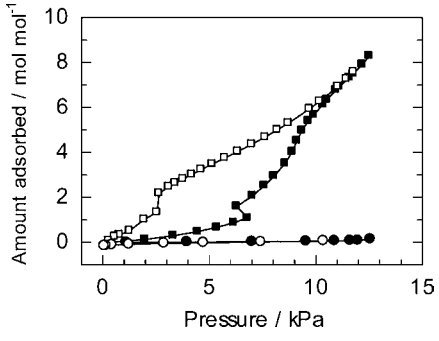

Figure 4. Adsorption (filled shapes) and desorption (open shapes) isotherms of methanol at 25 °C in **1** (● and ○) and **1′** (■ and □).

dx.doi.org/10.1021/ja4051668 | J. Am. Chem. Soc. 2013, 135, 11345−11350

process. The amount of methanol adsorbed at 10 kPa is approximately 6 mol per the chemical formula of **1′**, which corresponds to one methanol molecule per phosphate group in **1′**. We performed PXRD of **1′** under various pressure levels of methanol vapor at 25 °C to investigate the structure of **1′** with adsorbed methanol (**1′** ⊃ CH_3OH). The initial structure of **1′** is preserved after methanol adsorption (Figure S10 of the SI). The result indicates that methanol does not coordinate to the zinc center of **1′**, which would lead to another structural transformation because the coordination of methanol would cause deformation around the zinc ions. The pore of **1′** is specific for methanol and other gases such as N_2 (measured at 77 K); CO and CO_2 (measured at 195 K) were not adsorbed.

Modulation of the Proton Conductivity of 1′ by Methanol Adsorption. Methanol is known as a poor proton conductor compared with water.[18] So far, we have described the proton conduction path of **1′** in the low temperature region (1D zinc-phosphate chains) and its guest-accessible space. To demonstrate the dual functionality, we measured the proton conductivity of **1′** at 25 °C under different pressure levels of gaseous methanol [from 0 to 8 kPa, Figure 5 and Figure S11a

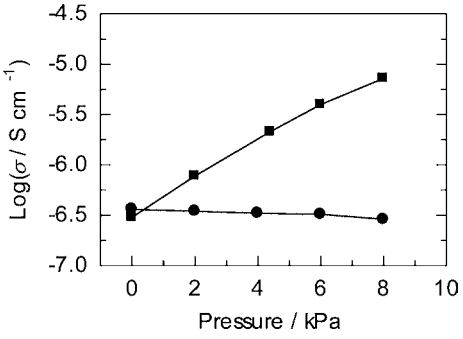

Figure 5. Proton conductivity of **1** (●) and **1′** (■) at 25 °C under various pressure levels of methanol vapor.

of the SI (Nyquist plots)]. At 0 kPa, the conductivity was 3.0×10^{-7} S cm^{-1}, which is close to the value under atmospheric N_2. The conductivity increased linearly with increasing methanol pressure. It eventually reached 7.3×10^{-6} S cm^{-1} at 8 kPa, which is 24 times higher than that at 0 kPa. This indicates that the methanol molecules are adsorbed in **1′** and enhance the conductivity. As a control experiment, we also measured the conductivity of **1** under increasing methanol pressure. In contrast to that of **1′**, the conductivity of **1** showed almost no dependence on pressure [Figure 5 and Figure S11b of the SI (Nyquist plots)]. The result is reasonable because **1** does not adsorb methanol at 25 °C. Thus, having the accessible space for methanol, the proton conductivity of **1′** is modulated by methanol adsorption.

Mechanism for Modulating the Proton Conductivity of 1′. We questioned how the adsorbed methanol interacts with the pore surface of **1′** to enhance the proton conductivity because methanol is usually a poor proton carrier. To investigate this point, we relied on solid-state NMR spectroscopy. The ^2H solid-state static NMR spectrum of **1′** ⊃ CD_3OH (prepared at 6 kPa) at 25 °C revealed the presence of host–guest interactions (Figure S12 of the SI). It shows a Pake doublet and a zero-frequency singlet, which represent interacting and free CD_3OH, respectively. The fitting of the spectrum revealed an effective quadrupole coupling constant (Q_{eff}) of 50 kHz and an asymmetry factor (η) of 0.048 for the Pake doublet. The values of Q_{eff} and η indicate the presence of rigidly bound CD_3 groups rapidly reorienting only around their 3-fold symmetry (C_3) axis.[19] Hence we speculate that there are rigid hydrogen-bonding interactions between **1′** and methanol.

The $^1H-^{13}C$ heteronuclear correlation (HETCOR) NMR technique, which highlights spatially adjacent species, was used to confirm the host–guest interaction at the atomic level. Figure 6 shows the 2D spectrum of **1′** ⊃ $^{13}CH_3OH$. In the ^{13}C

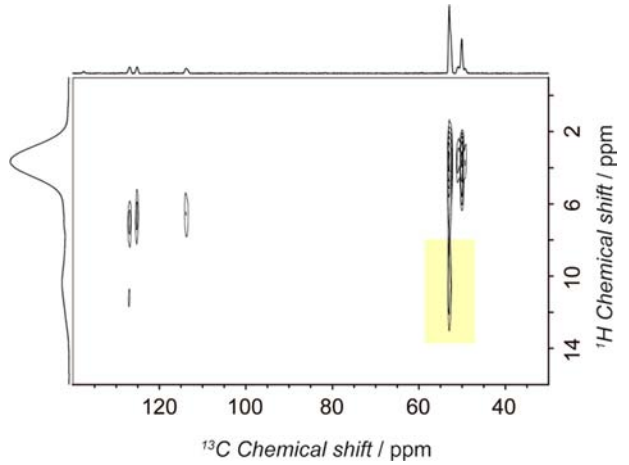

Figure 6. $^1H-^{13}C$ HETCOR NMR spectrum of **1′** ⊃ $^{13}CH_3OH$. The correlation peak between the methyl carbon at 53 ppm and the phosphate proton at 11 ppm is highlighted by the yellow box.

projection, we observed chemical shifts for methanol at 50 and 53 ppm, which is consistent with the result from the ^2H NMR spectrum discussed above. Considering the fact that liquid methanol shows a ^{13}C NMR peak at 48 ppm, the peak at 53 ppm likely represents methanol interacting with **1′**. The ^{13}C peaks of Hbim were observed around 120 ppm. In the ^1H projection of Hbim, the peak at 3 ppm was assigned to the methyl protons and that at 7 ppm, the phenyl protons. These assignments were supported by the $^1H-^{13}C$ correlation peaks for the methyl carbon and the carbons of Hbim, respectively. Therefore, the peak at 11 ppm could be assigned to the hydroxyl groups of the phosphate moieties of **1′**, which is reasonable for $H_2PO_4^-$.[20] The correlation peak between the interacting methyl carbon at 53 ppm and the phosphate proton at 11 ppm, highlighted in yellow in Figure 6, gives the most important insight for understanding the host–guest interaction. This correlation peak indicates that the methanol and phosphate residues are spatially adjacent. Therefore, we conclude that the phosphate moieties of **1′** form a hydrogen bond with methanol, which enables modulation of the proton conductivity of **1′**. The methanol molecules adsorbed in **1′** positively influence the conductivity through hydrogen-bond interactions (Scheme 1).

■ CONCLUSIONS

Here we present a new synthetic strategy for preparing a dual-function proton conductor involving the creation of an intrinsic proton conductor with guest-accessible space as a coordination polymer. We adopted a proton conductive ligand ($H_2PO_4^-$) as well as a bulky template (Hbim) to synthesize the coordination polymer $[Zn_3(H_2PO_4)_6(H_2O)_3](Hbim)$ (**1**). Its dehydrated state, $[Zn_3(HPO_4)_6](Hbim)$ (**1′**) shows intrinsic proton conductivity that is higher than **1** because of the rearranged

dx.doi.org/10.1021/ja4051668 | J. Am. Chem. Soc. 2013, 135, 11345–11350

Scheme 1. Schematic Representation of the Interaction between Methanol and 1′ Suggested by the ^{2}H Static and $^{1}H-^{13}C$ HETCOR NMR Spectra[a]

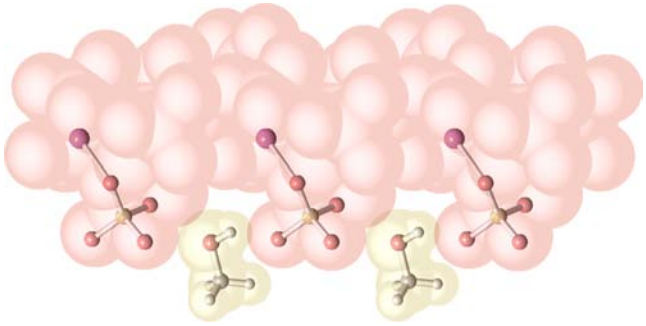

[a]The atoms Zn, P, O, N, C, and H are shown in purple, yellow, red, blue, gray, and white, respectively.

hopping path and quasi-liquid mobility of the benzimidazole moiety. The dehydrated framework **1′** shows intrinsic proton conductivity as high as 1.3×10^{-3} S cm^{-1} at 120 °C and also exhibits porosity, enabling the adsorption of gaseous methanol, features representative of its dual functionality. The in situ adsorption of methanol improves the proton conductivity of **1′** by 24 times, despite the poor proton-conductive nature of methanol. The methanol residues in the pore of **1′** form hydrogen-bond interactions with the phosphate moieties and contribute to proton conduction through the interactions. This coordination-polymer-based dual-function proton conductor is an interesting construct for the development of a new class of sensors and catalysts.

EXPERIMENTAL SECTION

Synthesis of $[Zn_3(H_2PO_4)_6(H_2O)_3](Hbim)$ (1). All chemicals and solvents used in the syntheses were of reagent grade and used without further purification. Zinc oxide (243 mg, 3 mmol), benzimidazole (118 mg, 1 mmol), phosphoric acid (85% in H_2O, 402 μL, 6 mmol) were put into a 10 mL Teflon jar with two steel-cored 10 mm teflone balls. The mixture was ground for 60 min in a Retch MM200 grinder mill operating at 25 Hz. The powder obtained was washed by methanol and evacuated at ambient temperature overnight to get dry **1** in pure phase. The single crystal of **1** was grown from the mixture of the same reagents without milling. Zinc oxide, benzimidazole, and phosphoric acid are contacted at room temperature, and a single crystal was grown at the solid–liquid interface. Deuterated **1**-P-d_2 and **1**-Hbim-d_4 were obtained using deuterated phosphoric acid (85% in D_2O) and benzoimidazole-4,5,6,7-d_4 instead of normal phosphoric acid and benzimidazole, respectively. **1′** is obtained by evacuating **1** at 100 °C for 3 h.

General Methods. The single crystal X-ray diffraction measurement were performed at 223 K with a Rigaku AFC10 diffractometer with Rigaku Saturn Kappa CCD system equipped with a MicroMax-007 HF/VariMax rotating-anode X-ray generator with confocal monochromated MoKα radiation. The data were processed by a direct method (SIR97) and refined by full-matrix least-squares refinement using the SHELXL-97 computer program. The thermogravimetric analysis (TGA) was obtained using a Rigaku TG8120 under flowing nitrogen with 10 K min^{-1} ramp rate. The powder X-ray diffraciton (PXRD), variable temperature PXRD, and PXRD under methanol vaor were collected on a Rigaku RINT 2200 Ultima diffractometer with CuKα anode. The differential scanning calorimetry (DSC) was carried out with a Mettler Toledo DSC822e/200 at the heating rate of 10 K min^{-1}. The infrared (IR) Spectroscopy was obtained using a Nicolet ID5 ATR operating at ambient temperature. The solid state ^{31}P CPMAS, ^{2}H static, and $^{1}H-^{13}C$ HETCOR NMR spectra were recorded on a Bruker ADVANCE 400 MHz spectrometer. The spinning rate for CPMAS and HETCOR spectra was 14 kHz. ^{2}H spectra were recorded using a quadrupole echo pulse sequence. The synchrotron powder X-ray diffraction for Pawley fitting were measured by the synchrotron radiation (λ = 0.8 Å) with the large Debye–Scherrer camera and imaging plate as detectors on the BL02B2 beamline at the Super Photon Ring (SPring-8). The face index was performed by X-Cell computer program. Reflex module of Materials Studio was used for the Pawley fitting analysis and unit cell refinement. The adsorption isotherms of gaseous methanol were measured by using a Belsorp-aqua.

Conductivity Measurement. The impedance analysis was performed on powders of **1** and **1′** without modification. The powders (ca. 50 mg) were pressed at 1000 kgf for 2 min by a standard 5 mm die and sandwiched between two gold electrodes. The impedance cell was filled with dry N_2 at atmospheric pressure or gaseous methanol from 0 to 8 kPa. The measurements were done at thermal equilibrium by holding for 30 mitutes at each measuring temperature. The measurements were performed using an impedance and gain-phase analyzer (Solartron SI 1260 Impedance/Gain-Phase analyzer) over the frequency range 1 Hz–1 MHz with an input voltage amplitude of 30 mV. ZView software was used to fit impedance data sets by means of an equivalent circuit simulation to obtain the resistance values.

ASSOCIATED CONTENT

Supporting Information

IR spectra, TGA, PXRD, ^{31}P CPMAS, and ^{2}H static solid-state NMR spectra, Pawley fitting analysis, Nyquist plots, and DSC. This material is available free of charge via the Internet at http://pubs.acs.org.

AUTHOR INFORMATION

Corresponding Author

horike@sbchem.kyoto-u.ac.jp; kitagawa@icems.kyoto-u.ac.jp

Notes

The authors declare no competing financial interest.

ACKNOWLEDGMENTS

This work was supported by the PRESTO Program of the Japan Science and Technology Agency (JST), and a Grant-in-Aid for Scientific Research on the Innovative Areas: “Fusion Materials” from the Ministry of Education, Culture, Sports, Science and Technology (MEXT), Japan. iCeMS is supported by the World Premier International Research Initiative (WPI), MEXT, Japan.

REFERENCES

(1) (a) Iwahara, H.; Esaka, T.; Uchida, H.; Yamauchi, T.; Ogaki, K. *Solid State Ionics* **1986**, *18–19* (Part 2), 1003. (b) Yajima, T.; Koide, K.; Fukatsu, N.; Ohashi, T.; Iwahara, H. *Sens. Actuators, B* **1993**, *14*, 697. (c) Kreuer, K. D. *Chem. Mater.* **1996**, *8*, 610.

(2) Kudo, T.; Fueki, K. *Solid State Ionics*; Wiley-VCH: New York, 1990.

(3) (a) Alberti, G.; Casciola, M. *Solid State Ionics* **1997**, *97*, 177. (b) Yoon, M.; Suh, K.; Natarajan, S.; Kim, K. *Angew. Chem., Int. Ed.* **2013**, *52*, 2688.

(4) (a) Evans, O. R.; Lin, W. B. *Acc. Chem. Res.* **2002**, *35*, 511. (b) Yaghi, O. M.; O'Keeffe, M.; Ockwig, N. W.; Chae, H. K.; Eddaoudi, M.; Kim, J. *Nature* **2003**, *423*, 705. (c) Kitagawa, S.; Kitaura, R.; Noro, S. *Angew. Chem., Int. Ed.* **2004**, *43*, 2334. (d) Cheetham, A. K.; Rao, C. N. R.; Feller, R. K. *Chem. Commun.* **2006**, *0*, 4780. (e) Ferey, G. *Chem. Soc. Rev.* **2008**, *37*, 191. (f) Shimizu, G. K. H.; Vaidhyanathan, R.; Taylor, J. M. *Chem. Soc. Rev.* **2009**, *38*, 1430. (g) Farha, O. K.; Hupp, J. T. *Acc. Chem. Res.* **2010**, *43*, 1166. (h) Zhang, J. P.; Zhang, Y. B.; Lin, J. B.; Chen, X. M. *Chem. Rev.* **2012**, *112*, 1001.

(5) (a) Nagao, Y.; Fujishima, M.; Ikeda, R.; Kanda, S.; Kitagawa, H. *Inorg. Chem. Commun.* **2003**, *6*, 346. (b) Bureekaew, S.; Horike, S.; Higuchi, M.; Mizuno, M.; Kawamura, T.; Tanaka, D.; Yanai, N.; Kitagawa, S. *Nat. Mater.* **2009**, *8*, 831. (c) Hurd, J. A.; Vaidhyanathan, R.; Thangadurai, V.; Ratcliffe, C. I.; Moudrakovski, I. L.; Shimizu, G. K. *Nat. Chem.* **2009**, *1*, 705. (d) Sadakiyo, M.; Yamada, T.; Kitagawa, H. *J. Am. Chem. Soc.* **2009**, *131*, 9906. (e) Ohkoshi, S.; Nakagawa, K.; Tomono, K.; Imoto, K.; Tsunobuchi, Y.; Tokoro, H. *J. Am. Chem. Soc.* **2010**, *132*, 6620. (f) Taylor, J. M.; Mah, R. K.; Moudrakovski, I. L.; Ratcliffe, C. I.; Vaidhyanathan, R.; Shimizu, G. K. H. *J. Am. Chem. Soc.* **2010**, *132*, 14055. (g) Pardo, E.; Train, C.; Gontard, G.; Boubekeur, K.; Fabelo, O.; Liu, H.; Dkhil, B.; Lloret, F.; Nakagawa, K.; Tokoro, H.; Ohkoshi, S.; Verdaguer, M. *J. Am. Chem. Soc.* **2011**, *133*, 15328. (h) Sahoo, S. C.; Kundu, T.; Banerjee, R. *J. Am. Chem. Soc.* **2011**, *133*, 17950. (i) Shigematsu, A.; Yamada, T.; Kitagawa, H. *J. Am. Chem. Soc.* **2011**, *133*, 2034. (j) Umeyama, D.; Horike, S.; Inukai, M.; Hijikata, Y.; Kitagawa, S. *Angew. Chem., Int. Ed.* **2011**, *50*, 11706. (k) Colodrero, R. M. P.; Olivera-Pastor, P.; Losilla, E. R.; Hernández-Alonso, D.; Aranda, M. A. G.; Leon-Reina, L.; Rius, J.; Demadis, K. D.; Moreau, B.; Villemin, D.; Palomino, M.; Rey, F.; Cabeza, A. *Inorg. Chem.* **2012**, *51*, 7689. (l) Jeong, N. C.; Samanta, B.; Lee, C. Y.; Farha, O. K.; Hupp, J. T. *J. Am. Chem. Soc.* **2012**, *134*, 51. (m) Ponomareva, V. G.; Kovalenko, K. A.; Chupakhin, A. P.; Dybtsev, D. N.; Shutova, E. S.; Fedin, V. P. *J. Am. Chem. Soc.* **2012**, *134*, 15640. (n) Panda, T.; Kundu, T.; Banerjee, R. *Chem. Commun.* **2013**, *49*, 6197.

(6) (a) Horike, S.; Umeyama, D.; Inukai, M.; Itakura, T.; Kitagawa, S. *J. Am. Chem. Soc.* **2012**, *134*, 7612. (b) Umeyama, D.; Horike, S.; Inukai, M.; Itakura, T.; Kitagawa, S. *J. Am. Chem. Soc.* **2012**, *134*, 12780.

(7) Vilčiauskas, L.; Tuckerman, M. E.; Bester, G.; Paddison, S. J.; Kreuer, K. D. *Nature Chem.* **2012**, *4*, 461.

(8) In the crystal structure refinement of **1**, we could not find electron densities for hydrogen atoms except for those of coordinated water molecules. The hydrogen atoms on oxygen atoms of phosphate and those on nitrogen atoms of Hbim are likely too disordered to be located. Thus we locate hydrogen atoms only for the coordinated water molecules (DFIX, 0.95 Å, σ = 0.02) and for carbon atoms of Hbim (HFIX 43). Hydrogen atoms of the phosphates are supposed to be present between their oxygen atoms that are in a distance of hydrogen bond.

(9) Agmon, N. *Chem. Phys. Lett.* **1995**, *244*, 456.

(10) (a) Hayashi, S.; Hayamizu, K. *Bull. Chem. Soc. Jpn.* **1989**, *62*, 3061. (b) Reinert, P.; Logar, N. Z.; Patarin, J.; Kaucic, V. *Eur. J. Solid State Inorg. Chem.* **1998**, *35*, 373. (c) Akamatsu, T.; Kasuga, T.; Nogami, M. *Adv. Mater. Res.* **2007**, *15*−*17*, 327.

(11) Barsoukov, E.; Macdonald, J. R. *Impedance Spectroscopy*; Wiley-Interscience: New York, 2005.

(12) (a) Bauerle, J. E. *J. Phys. Chem. Solids* **1969**, *30*, 2657. (b) Hooper, A. *J. Phys. D: Appl. Phys.* **1977**, *10*, 1487.

(13) Guo, X.; Ding, Y. *J. Electrochem. Soc.* **2004**, *151*, J1.

(14) (a) Kundu, T.; Sahoo, S. C.; Banerjee, R. *Chem. Commun.* **2012**, *48*, 4998. (b) Mallick, A.; Kundu, T.; Banerjee, R. *Chem. Commun.* **2012**, *48*, 8829.

(15) (a) Schmidt-Rohr, K.; Spiess, H. *Multidimensional Solid-State NMR and Polymers*; Academic Press: New York, 1994; (b) Lee, Y. J.; Murakhtina, T.; Sebastiani, D.; Spiess, H. W. *J. Am. Chem. Soc.* **2007**, *129*, 12406.

(16) Merinov, B. V.; Chisholm, C. R. I.; Boysen, D. A.; Haile, S. M. *Solid State Ionics* **2001**, *145*, 185.

(17) Ivanova, I. I.; Kolyagin, Y. G. *Chem. Soc. Rev.* **2010**, *39*, 5018.

(18) (a) Conway, B. E.; Bockris, J. O.; Linton, H. *J. Chem. Phys.* **1956**, *24*, 834. (b) Quigley, E. P.; Emerick, A. J.; Crumrine, D. S.; Cukierman, S. *Biophys. J.* **1998**, *75*, 2811.

(19) (a) Takahashi, S.; Nakato, T.; Hayashi, S.; Sugahara, Y.; Kuroda, K. *Inorg. Chem.* **1995**, *34*, 5065. (b) Horike, S.; Matsuda, R.; Kitaura, R.; Kitagawa, S.; Iijima, T.; Endo, K.; Kubota, Y.; Takata, M. *Chem. Commun.* **2004**, 2152.

(20) (a) Haile, S. M.; Liu, H.; Secco, R. A. *Chem. Mater.* **2003**, *15*, 727. (b) Yamada, K.; Sagara, T.; Yamane, Y.; Ohki, H.; Okuda, T. *Solid State Ionics* **2004**, *175*, 557.